Folding and Aggregation Kinetics of a β-Hairpin†

Victor Muñoz,‡,§ Rodolfo Ghirlando,|| Francisco J. Blanco,‡,⊥ Gouri S. Jas,‡,@ James Hofrichter,‡ and William A. Eaton*,‡

Laboratory of Chemical Physics and Laboratory of Molecular Biology, National Institute of Diabetes and Digestive and Kidney Diseases, National Institutes of Health, Bethesda, Maryland 20892-0520, and Department of Chemistry and Biochemistry and Center for Biomolecular Structure and Organization, University of Maryland, College Park, Maryland 20742

Received December 15, 2005; Revised Manuscript Received March 31, 2006

ABSTRACT: We have investigated the solution structure, equilibrium properties, and folding kinetics of a 17-residue β-hairpin-forming peptide derived from the protein ubiquitin. NMR experiments show that at 4 °C the peptide has a highly populated β-hairpin conformation. At protein concentrations higher than 0.35 mM, the peptide aggregates. Sedimentation equilibrium measurements show that the aggregate is a trimer, while NMR indicates that the β-hairpin conformation is maintained in the trimer. The relaxation kinetics in nanosecond laser temperature-jump experiments reveal a concentration-independent microsecond phase, corresponding to β-hairpin unfolding-refolding, and a concentration-dependent millisecond phase due to oligomerization. Kinetic modeling of the relaxation rates and amplitudes yields the folding and unfolding rates for the monomeric β-hairpin, as well as assembly and disassembly rates for trimer formation consistent with the equilibrium constant determined by sedimentation equilibrium. When the net charge on the peptides and ionic strength were taken into account, the rate of trimer assembly approaches the Debye−Smoluchowski diffusion limit. At 300 K, the rate of formation of the monomeric hairpin is $(17\ \mu s)^{-1}$, compared to rates of $(0.8\ \mu s)^{-1}$ to $(52\ \mu s)^{-1}$ found for other peptides. After using Kramers theory to correct for the temperature dependence of the pre-exponential factor, the activation energy for hairpin formation is near zero, indicating that the barrier to folding is purely entropic. Comparisons with previously measured rates for a series of hairpins are made to distinguish between zipper and hydrophobic collapse mechanisms. Overall, the experimental data are most consistent with the zipper mechanism in which structure formation is initiated at the turn, the mechanism predicted by the Ising-like statistical mechanical model that was developed to explain the equilibrium and kinetic data for the β-hairpin from protein GB1. In contrast, the majority of simulation studies favor a hydrophobic collapse mechanism. However, with few exceptions, there is little or no quantitative comparison of the simulation results with experimental data.

The β-hairpin is the simplest antiparallel β-sheet and one of the principal secondary structural elements of proteins. In contrast to the α-helix, there is relatively little experimental information about β-hairpins. The difficulty in studying them results from their low stability in isolation, a tendency to aggregate, and in most cases the lack of a suitable probe for kinetic studies with optical methods. The first investigation of the structure, thermodynamics, and kinetics of a β-hairpin was carried out on the 16-residue sequence that forms the C-terminal β-hairpin of the immunoglobulin binding domain of streptococcal protein G (protein GB1) (*1*, *2*). This peptide remains monomeric at high concentrations, which allowed its β-hairpin conformation to be established by NMR (*1*). Burial of the lone tryptophan in a stabilizing hydrophobic cluster results in a large increase in the fluorescent quantum yield, providing a sensitive probe of folding. Kinetic and equilibrium studies showed surprisingly simple behavior for the GB1 peptide, with only two populations of molecules, folded and unfolded (*2*−*4*). Its two-state behavior, its microsecond folding time, and the recognition that β-hairpin folding captures much of the same physics underlying folding of single-domain proteins have motivated investigations of the β-hairpin-forming GB1 peptide both by theory (*5*−*9*) and by numerous simulations (*10*−*47*). Moreover, simple Ising-like models, very similar to the statistical mechanical model originally used to explain the GB1 peptide results (*2*, *5*), have been remarkably successful in explaining relative folding rates of single-domain proteins (*48*−*51*).

Although there have been a number of experimental investigations of β-hairpin structure and stability since this initial study (*52*−*70*), as well as simulation studies on β-hairpin peptides other than the GB1 sequence (*71*−*83*),

† This research was supported by the Intramural Research Program of the National Institute of Diabetes and Digestive and Kidney Diseases. V.M. is a recipient of a Dreyfus New Faculty Award, a Packard Fellowship for Science and Engineering, and a Searle Scholarship.

* To whom correspondence should be addressed. Telephone: (301) 496-6030. E-mail: eaton@helix.nih.gov.

‡ Laboratory of Chemical Physics, National Institute of Diabetes and Digestive and Kidney Diseases, National Institutes of Health.

§ University of Maryland.

|| Laboratory of Molecular Biology, National Institute of Diabetes and Digestive and Kidney Diseases, National Institutes of Health.

⊥ Present address: Structural Biology and Biocomputing Program, Centro Nacional de Investigaciones Oncológicas (CNIO), Madrid E-28029, Spain.

@ Present address: Department of Chemistry and Biochemistry, Baylor University Sciences Building, Waco, TX 76706.

10.1021/bi052556a CCC: $33.50
Published on Web 05/18/2006

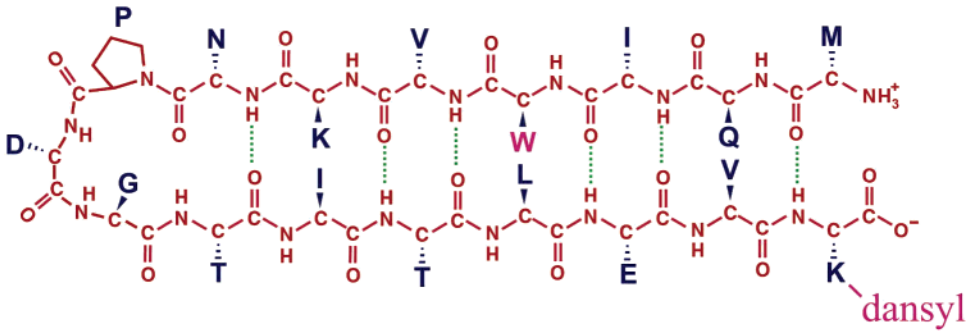

FIGURE 1: Schematic representation of β-hairpin structure. Tryptophan replaced the phenylalanine of the original ubiquitin sequence. The added dansylated lysine at the C-terminus interacts with the N-terminal methionine to further stabilize the hairpin structure.

there have been relatively few experimental kinetic studies (*84*−*89*). Consequently, it has not yet been possible to unambiguously determine by experiment which, if any, of the various mechanisms predicted by the theoretical and simulation studies is correct. In this work, we have used the laser temperature-jump technique to measure the kinetics of unfolding-refolding of a 17-residue peptide originating from the N-terminal β-hairpin of ubiquitin (Figure 1). Because the original hairpin is marginally stable in isolation, Searle et al. (*90*) replaced the five-residue bulged turn with the four-residue sequence that has a high turn propensity for a type I β-turn (NPDG). To create a fluorescent probe, we replaced the single phenylalanine of this modified sequence with tryptophan. However, experiments on this peptide showed undetectable fluorescence changes in kinetic experiments, suggesting a small change in the buried surface area upon hairpin formation and/or quenching in the folded conformation by the positively charged lysine that is two residues distant in the sequence. We therefore synthesized a peptide with a dansylated lysine added to the C-terminus. The dansyl group is an energy acceptor for tryptophan excitation and allowed hairpin formation to be monitored by changes in Förster resonance energy transfer (FRET) efficiency (Figure 1). An interesting complication is that the peptide aggregates, which we have investigated both by NMR and by sedimentation equilibrium studies.

MATERIALS AND METHODS

Samples. The peptide NH_2-MQIWVKNPDGTITLEVK-(dansyl)-COOH was purchased from California Peptide Research (Napa, CA) and was shown by HPLC and mass spectrometry to be >95% pure. The peptide was dissolved into a pH 10.5 sodium carbonate/bicarbonate buffer (50 mM).

NMR Experiments. NMR measurements were carried out on a Bruker DMX 500 MHz spectrometer. One- and two-dimensional spectra were recorded with peptide samples at concentrations of 0.035, 0.35, and 3.5 mM in 90% H_2O and 10% D_2O adjusted to pH 11.2 with concentrated NaOH. Water suppression was achieved through presaturation. At pH 11.2, only nonexchangeable protons were observed. In the absence of amide proton signals, assignment of resonances to particular protons in the peptide molecule was done on the basis of the spin system of unique residues (identified in TOCSY and DQF-COSY spectra) combined with the detection of sequential NOEs between aliphatic protons due to spin diffusion in NOESY spectra recorded with long mixing times and at different temperatures.

Sedimentation Equilibrium Experiments. Sedimentation equilibrium experiments were conducted on a Beckman Optima XL-A analytical ultracentrifuge at loading concentrations of 0.04, 0.35, and 3.5 mM and rotor speeds ranging from 26 000 to 50 000 rpm. Data were acquired as an average of 25 absorbance measurements at wavelengths of 250 (0.04 mM), 364 (0.35 mM), and 410 nm (3.5 mM) and a radial spacing of 0.001 cm. Data collected at 0.04 mM were analyzed in terms of a single ideal solute to obtain the buoyant molecular mass, $M_1(1 - \upsilon\rho)$, where υ is the partial molar specific volume and ρ is the solvent density. The temperature dependence of $M_1(1 - \upsilon\rho)$ was determined by collecting sedimentation equilibrium data for a 0.04 mM solution at 48 000 rpm at temperatures ranging from 4.0 to 25.0 °C. In all cases, analysis in terms of a single ideal solute yielded excellent fits with a random radial distribution of the residuals around zero (±0.02).

To measure the self-association equilibrium constants, experiments were carried out at three different loading concentrations (0.20, 0.31, and 0.48 mM) of the peptide, measuring at 364 nm, and with a rotor speed of 48 000 rpm. Data were collected at temperatures ranging from 4.0 to 25.0 °C. Simultaneous weighted nonlinear least-squares fitting of the data set at each temperature was performed using the function (*91*)

$$A_r = A_{0,1}\exp\left[M_1(1-\upsilon\rho)(r^2 - r_0^2)\frac{\omega^2}{2RT}\right] + A_{0,1}{}^n \exp\left[\ln k_{1,n} + nM_1(1-\upsilon\rho)(r^2 - r_0^2)\frac{\omega^2}{2RT}\right] \quad (1)$$

where n is the stoichiometry of the complex, $A_{0,1}$ is the absorbance at a reference point r_0 of the monomer, and $k_{1,n}$ is the monomer to n-mer self-association equilibrium constant on an absorbance concentration scale. Experimentally determined $M_1(1 - \upsilon\rho)$ values were used. These schemes have the equilibrium constant as a global fitting parameter and cell reference concentrations and baseline corrections as local fitting parameters. The simultaneous fitting of data from three different loading concentrations represents a stringent criterion for establishing the validity of the assumption that the system is indeed a reversibly self-associating system (*92*).

Using the extinction coefficient for the monomer, ϵ, the values of ln $k_{1,n}$ obtained experimentally were converted to ln $K_{1,n}$ values, where $K_{1,n}$ represents the association constant for the monomer to n-mer equilibrium on a molar concentration scale. The enthalpy, entropy, and heat capacity changes were obtained by fitting the data for an n of 3 with

$$-\ln K_{1,3} = \frac{\Delta H_0 - T\Delta S_0 + (T - T_0)\Delta C_p - T\Delta C_p \ln(T/T_0)}{RT} \quad (2)$$

where $K_{1,3} \equiv [T_{eq}]/[M_{eq}]^3$ and the reference temperature T_0 was taken to be 298 K. The equilibrium monomer concentration ($[M_{eq}]$) is the sum of the concentrations of the folded and (small fraction of) unfolded peptide (see below). To confirm the stoichiometry of the complex that was formed, data were collected at 34 000 rpm and a loading concentration of 3.5 mM. Due to the presence of higher-order aggregates, data were best fit in terms of two noninteracting ideal solutes.

Kinetic Experiments. Steady state fluorescence spectra were measured with a SPEX Fluorolog-2 spectrofluorimeter (model F1T11I). The laser temperature-jump instrument used in kinetics experiments has been described in detail previously (*93*). Briefly, the fundamental of a Q-switched Nd:YAG laser at 1064 nm was Raman-shifted in a high-pressure cell of methane to produce a ~5 ns, ~10 mJ pulse at 1540 nm. To obtain more uniform heating, the 1540 nm pulse was first split using a 50:50 beam splitter and focused onto the same spot from opposite sides of the sample (0.05 cm × 1 cm × 4.5 cm) cuvette. The delay between these two pulses was ~5 ns, so the total duration of the heating pulses was ~10 ns. The probe source for continuous excitation of tryptophan was an intracavity frequency-doubled argon ion laser (Coherent Innova 300) operating at 264 nm. The fluorescence was filtered with a 320−400 nm band-pass filter, collected at 90° with an end-on photomultiplier tube (Hamamatsu R6427), and recorded using a transient digitizer (Tektronix TDS 620). In a typical experiment, temperature jumps of 10−12 K were obtained, and a single kinetic trace was measured by averaging the curves from 3000 laser shots; the laser operated at 1.66 Hz to allow thermal diffusion out of the ~0.5 mm to be completed prior to the next heating pulse. The temperature increase was determined by measuring the change in fluorescence of N-acetyl-tryptophanamide (NATA) at each initial temperature under identical experimental conditions before and after collecting data on a peptide. Band-pass filters were used to isolate the fluorescence from tryptophan or dansyl. To minimize photodamage, a shutter, which remained open only during collection of a kinetic trace associated with each heating pulse, i.e., ~5 ms, was inserted in front of this UV probe laser. Also, solutions were degassed by aspiration to reduce cavitation.

Analysis of Kinetics. The second-order rate equations of the kinetic model

$$3U \underset{k_{-1}}{\overset{k_1}{\rightleftharpoons}} H_A + H_B + H_C \underset{k_{-2}}{\overset{k_2}{\rightleftharpoons}} (H_AH_B/3 + H_BH_C/3 + H_CH_A/3) + M \underset{k_{-3}}{\overset{k_3}{\rightleftharpoons}} H_AH_BH_C$$

were linearized, which assumes that the perturbation from the temperature jump was sufficiently small that squared concentration displacement terms could be neglected. The equilibrium populations as a function of the final (elevated) temperature were calculated by finding the physically meaningful root of the third-degree equation

$$[P]_{total} = [M_{eq}] + \frac{k_1}{k_{-1}}[M_{eq}] + \frac{2k_2}{k_{-2}}[M_{eq}]^2 + \frac{3k_2k_3}{k_{-2}k_{-3}}[M_{eq}]^3 \quad (3)$$

where the rate coefficients and equilibrium populations are related by

$$\frac{k_1}{k_{-1}} = \frac{[M_{eq}]}{[U_{eq}]}; \quad \frac{k_2}{k_{-2}} = \frac{[D_{eq}]}{[M_{eq}]^2}; \quad \frac{k_3}{k_{-3}} = \frac{[T_{eq}]}{[M_{eq}][D_{eq}]} \quad (4)$$

where M is $H_A/3 + H_B/3 + H_C/3$, D is $H_AH_B/3 + H_BH_C/3 + H_CH_A/3$, and T is $H_AH_BH_C$.

Using these equilibrium populations at the final temperature and the linearization method, the system of four differential equations can be solved by finding the eigenvalues and eigenvectors of the rate matrix **K**:

$$\mathbf{K} = \begin{bmatrix} -k_1 & k_{-1} & 0 & 0 \\ k_1 & -(k_{-1} + 4k_2[M_{eq}] + k_3[D_{eq}]) & 2k_{-2} - k_3[M_{eq}] & 3k_{-3} \\ 0 & 2k_2[M_{eq}] - k_3[D_{eq}] & -(k_{-2} + k_3[M_{eq}]) & 3k_{-3} \\ 0 & k_3[D_{eq}] & k_3[M_{eq}] & -3k_{-3} \end{bmatrix} \quad (5)$$

in which there is a symmetry factor of 3 multiplying the trimer off-rate (k_{-3}) to account for the fact that the trimer can be broken in three different ways. The quantum yield of tryptophan as a function of temperature was measured in the peptide without dansylated lysine. The relative tryptophan quantum yields for each of the four species in the kinetic model are simply obtained using Förster's theory from the tryptophan quantum yield, the characteristic donor acceptor average distance (see Table 1), and an R_o of 2.1 nm for the tryptophan−dansyl pair at pH 10. The quantum yield of dansyl in the unfolded hairpin was assumed to be identical to that of free dansyllysine. The quantum yields of dansyl in the other three species are listed in Table 1.

RESULTS

Conformation from NMR. To establish the properties of the folded structure of the ubiquitin-derived peptide, we studied its conformational properties at a low temperature (273 K) using two-dimensional ^{1}H NMR spectroscopy. As shown in Figure 2A, the pattern of conformational shifts of α-carbon protons is very similar to that reported by Searle et al. (*90*) on the peptide without the substitution of phenylalanine with tryptophan and without the addition of a dansylated lysine. The differences in patterns are localized in specific residues (Figure 2A) and could be explained as arising from differential ring current effects between the original phenylalanine and the new tryptophan together with additional ring current effects from the incorporated dansyl (i.e., the N-terminal methionine that faces the dansyllysine in the hairpin structure). Furthermore, the same interstrand α-proton NOEs are observed (Figure 2B). NOEs occur between the α-protons of residues 6 and 12, 4 and 14, and 2 and 16, demonstrating that the register of the strands is the same as that found by Searle et al. (*90*) and that the hairpin conformation extends to the N- and C-termini. Hydrophobic interactions between the N-terminal methionine

Table 1: Parameters of the Kinetic Model[a]

Rate Constants at 298 K and Apparent Activation Energies [obtained using the rate expression $k = k_0 \exp(-E_a/RT)$]		
	rate coefficient	E_a (kcal/mol)
k_1	$(4.8 \pm 1.5) \times 10^4$ s^{-1}	4.0 ± 0.5
k_{-1}	$(1.1 \pm 0.2) \times 10^4$ s^{-1}	9.5 ± 1.0
k_2	$(1.3 \pm 0.7) \times 10^8$ M^{-1} s^{-1}	-3.3 ± 1.0
k_{-2}	$(6.8 \pm 1.9) \times 10^7$ s^{-1}	8.2 ± 0.3
k_3	$(1.3 \pm 0.7) \times 10^8$ M^{-1} s^{-1}	-3.3 ± 1.0
k_{-3}	$(6.1 \pm 3.4) \times 10^1$ s^{-1}	16.4 ± 0.5
Dansyl Quantum Yields		
unfolded monomer (U)		0.034
monomeric hairpin (M)		0.30 ± 0.15
hairpin dimer and trimer (D, T)		0.46 ± 0.25
Average Tryptophan−Dansyl Distances (nm)		
unfolded monomer (U)[b]		2.2 ± 0.8
monomeric hairpin (M)		1.1 ± 0.2
hairpin dimer and trimer (D, T)		1.5 ± 0.6

[a]The uncertainty in each parameter is defined as the change that increases the sum of squared residuals by $(N - m + 1)/(N - m)$, where N is the number of data points and m is the number of parameters necessary to calculate the data points. [b] For simplicity, no account was taken of the distance distribution in the unfolded peptide.

and the dansyl group may be responsible for the observation of little or no fraying.

The NMR lines broadened with an increase in concentration from 0.035 to 3.5 mM, signaling peptide aggregation. The conformational shifts of the α-protons at 3.5 mM were similar to those at 0.35 mM but slightly increased, suggesting a stabilization of the hairpin structure. The same set of long-range NOEs that define the strand pairing was observed at both concentrations. With the increased sensitivity of the higher concentration, additional weak NOEs were observed. All these new NOEs were compatible with the hairpin structure except for one weak NOE between the side chains of residues 4 and 13, which are located in opposite faces of the hairpin structure. The 4−13 NOE might arise from a minor distorted conformer in fast equilibrium with the regular hairpin and other disordered conformations.

Equilibrium Thermal Unfolding from FRET. The stability of the hairpin was investigated from the temperature dependence of the FRET efficiency (Figure 3). To prevent aggregation, these experiments were carried out at peptide concentrations of 10 μM. It is not possible to extract accurate equilibrium constants from these curves because the spectroscopic values for the completely unfolded hairpin are unknown. The curves do show, however, that the midpoint temperature of the unfolding curve is higher than ∼335 K. The similarity of the NMR (data not shown) and FRET efficiency unfolding curves suggests this hairpin folds and unfolds in a two-state process, but additional experiments will be required to establish this with certainty.

Molecular Weights and Aggregation from Sedimentation Equilibrium. To characterize the aggregation process, we carried out sedimentation equilibrium experiments at different peptide concentrations. A 0.04 mM solution of the peptide was studied at 4.0 °C and rotor speeds from 42 000 to 50 000 rpm. In all cases, the data were adequately modeled in terms of a single ideal solute (Figure 4); the peptide appears to be monodisperse, as identical values of the buoyant molecular mass [$M_1(1 - \upsilon\rho) = 575 \pm 5$ g/mol] were obtained at different rotor speeds. Using a partial specific volume of

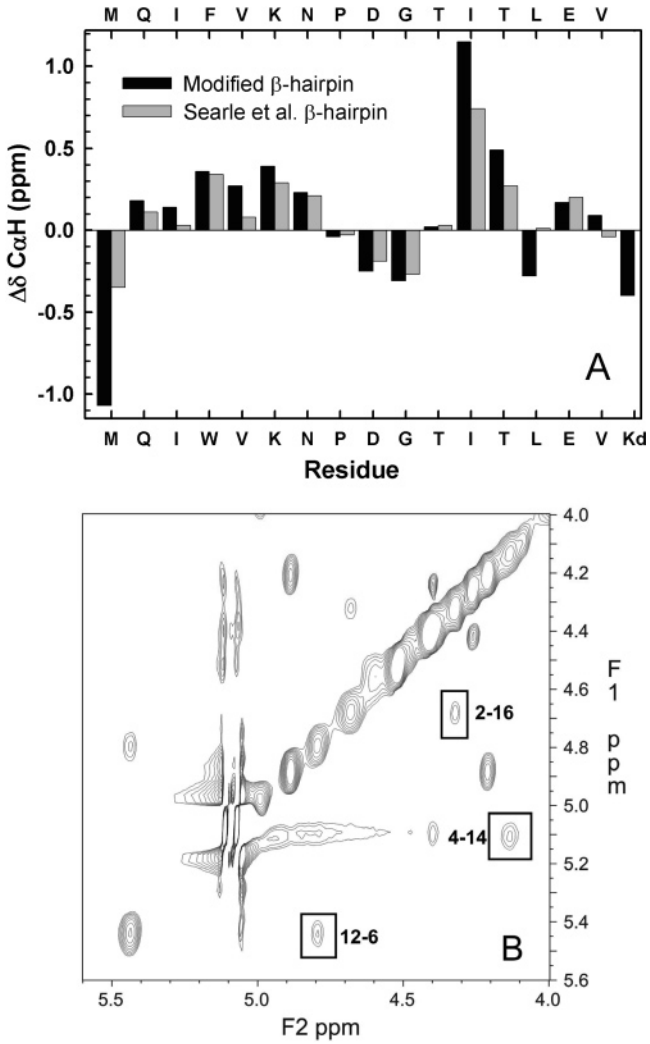

FIGURE 2: NMR results. (A) Conformational shifts of α-carbon protons. The differences between the chemical shifts observed for the α-carbon protons and those of a random coil (*112*). The black bars correspond to the molecule in Figure 1 at 273 K and pH 11.2 (its amino acid sequence is shown at the bottom with Kd signifying dansyllysine) and the gray bars to the molecule studied by Searle et al. at pH 3.5 and 278 K (its sequence is shown at the top) (*90*). Positive values (upfield shifts) correspond to strand conformation, while the negative value (downfield shift) signals the center of the turn at aspartate 9. The low value at leucine 14 presumably results from ring current effects of the opposing tryptophan or phenyalanine. (B) Interstrand backbone NOEs. Portion of the 150 ms NOESY spectrum showing the three $C_\alpha H - C_\alpha H$ NOEs that define strand pairing.

0.757 cm^3/g at 25.0 °C, calculated on the basis of the amino acid composition (*94*), assuming an average $d\upsilon/dT$ of 4.25×10^{-4} cm^3 g^{-1} K^{-1} (*95*) and a calculated solution density of 1.0055 g/cm^3, this corresponds to an experimental molecular mass of 2310 ± 20 g/mol. This value is close to the expected monomer molecular mass of 2204 g/mol. The buoyant molecular mass of the peptide was determined as a function of the temperature, at a single rotor speed of 48 000 rpm, and the corresponding partial specific volumes were determined. In the temperature range of 4.0−25.0 °C, υ varied linearly with temperature (data not shown) with a $d\upsilon/dT$ of $(8.3 \pm 0.6) \times 10^{-4}$ cm^3 g^{-1} K^{-1}. On the basis of this experimental value of $d\upsilon/dT$, an experimental molecular mass at 4.0 °C of 2235 ± 20 g/mol is thus determined. We note that the value of $d\upsilon/dT$ determined here is larger than typical

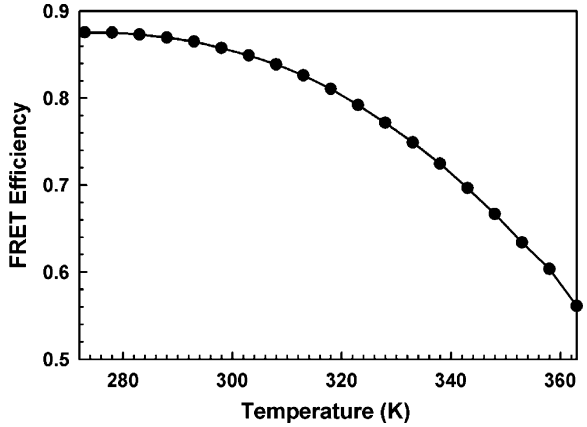

FIGURE 3: Equilibrium unfolding curve. The FRET efficiency is plotted vs temperature. The FRET efficiency (E) was calculated at each temperature from the relation $E = 1 - I_{DA}/I_D$, where I_{DA} is the tryptophan fluorescence intensity integrated from 300 to 450 nm for the dansylated peptide and I_D is the corresponding intensity for the peptide without the dansylated lysine.

values yet within the range of reported values (*95*).

Sedimentation equilibrium studies of a 0.35 mM solution at rotor speeds ranging from 42 000 to 50 000 rpm resulted in absorbance profiles that could not be modeled in terms of a single ideal solute. This, coupled with the fact that force fitting in terms of a single ideal solute returns a weight average buoyant molecular mass of 850 g/mol, indicates that the peptide self-associates. To determine the stoichiometry and association constants of the higher-order complexes as well as to demonstrate the reversibility of the self-association, experiments were carried out at three different loading concentrations (0.20, 0.31, and 0.48 mM). Data collected at 4.0 °C were analyzed in terms of various self-association schemes (eq 1) with stoichiometries (n) ranging from 2 to 6. Best fits were obtained with an n of 3, resulting in a ln k_3 of 0.053 ± 0.008 (Figure 4). The formation of mixed complexes was also considered. In models where both trimers and n-mers are formed, the data fit returns ln $k_{1,3}$ values of 0.053 and ln $k_{1,n}$ values of less than ~70, demonstrating that the peptide self-associates solely into trimers. Identical observations were made for data collected in the range of 7.0−25.0 °C. Accordingly, we analyzed all of the data in terms of a monomer ⇌ trimer equilibrium to obtain values of $K_{1,3}$. A plot of ln$K_{1,3}$ versus the reciprocal absolute temperature shows considerable curvature, indicating a significant heat capacity change (Figure 5). Fitting eq 2 to the data yields the following thermodynamic parameters: $\Delta H_0 = -10.4 \pm 1.7$ kcal/mol, $\Delta S_0 = -7.3 \pm 5.6$ cal mol^{-1} K^{-1}, $T_0 = 298$ K, and $\Delta C_p = -760 \pm 150$ cal mol^{-1} K^{-1}. Interestingly, the ΔC_p for association and dissociation of the trimer is very similar to that expected for the folding and unfolding of a protein of the same size [i.e., 13.9 cal mol^{-1} K^{-1} residue^{-1} (*96*) × 51 residues].

A series of sedimentation equilibrium experiments were carried out on a sample loaded at a concentration of 3.5 mM. At this elevated concentration, the peptide was expected to be wholly trimeric. Data collected at 4.0 °C and 34 000 rpm show a clear biphasic pattern, indicating the presence of two species (data not shown). Analysis in terms of two noninteracting solutes resulted in buoyant molecular masses of 1720 ± 50 and 18 200 ± 800 g/mol, the former being exactly 3 times the value for the monomer, determined at a 100-fold lower concentration, and the latter corresponding to a molecular mass of 69 700 ± 3000 g/mol, indicating further aggregation. Examination of these higher-order aggregates by atomic force microscopy showed only amorphous material, and no evidence of fibrils.

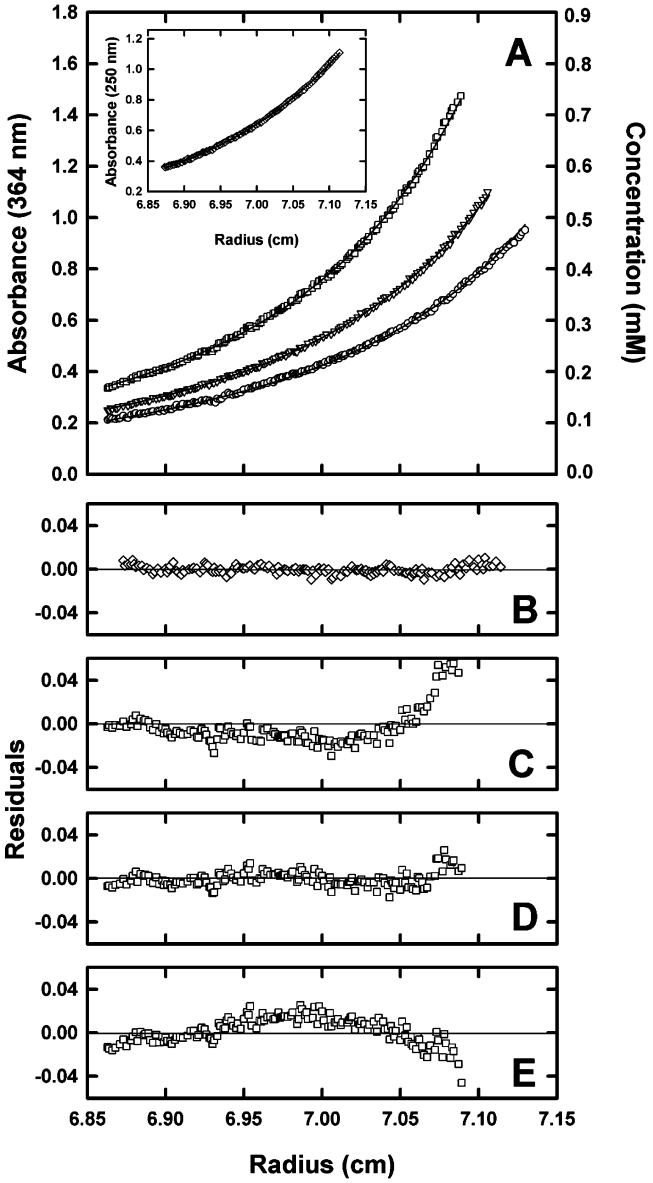

FIGURE 4: Sedimentation equilibrium data. (A) Sedimentation equilibrium profiles at 364 nm and 48 000 rpm. Experiments were performed at three different loading concentrations: 0.20 (○), 0.31 (▽), and 0.48 mM (□). The lines through the data are the best fit for a reversible monomer ⇌ trimer self-association. The inset shows the profile at 250 nm and 50 000 rpm for a sample loaded at 0.04 mM. (B) Distribution of residuals at 0.04 mM assuming a single species. (C) Residuals at 0.20 mM from the parameters obtained from simultaneous fits assuming a monomer ⇌ dimer equilibrium. (D) Same as panel C for a monomer ⇌ trimer equilibrium. (E) Same as panel C for a monomer ⇌ tetramer equilibrium. The fits for monomer−pentamer and higher-order aggregates were much worse.

Folding and Aggregation Kinetics. The kinetics of unfolding-folding was measured from the change in fluorescence of both the tryptophan and the dansyl group following a nanosecond laser temperature jump (Figure 6). The initial experiments were carried out at a peptide concentration of 1.1 mM. After a very rapid (<10 ns) decrease, the tryptophan fluorescence increases in a microsecond process, indicating

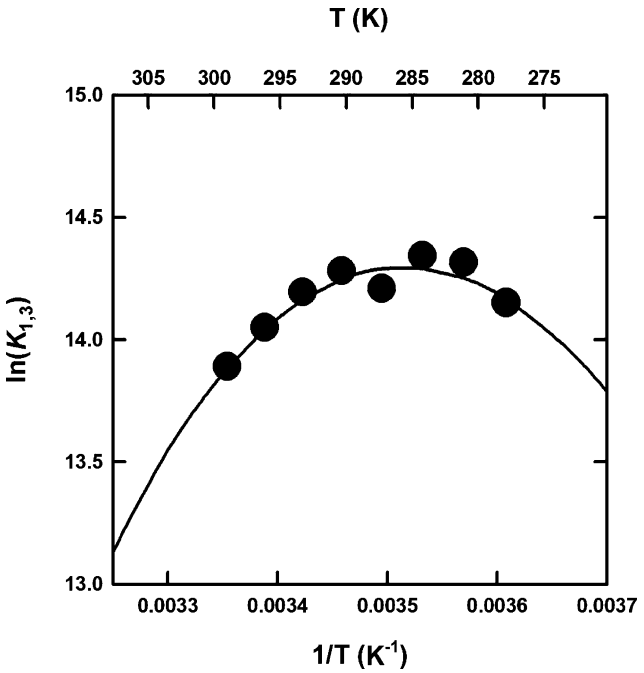

FIGURE 5: Temperature dependence of the monomer ⇌ trimer equilibrium constant determined from sedimentation equilibrium data. The curve is calculated from eq 2 with the following thermodynamic parameters: $T_0 = 298$ K, $\Delta H_0 = -10.4$ kcal/mol, $\Delta S_0 = -7.3$ cal mol^{-1} K^{-1}, and $\Delta C_p = -760$ cal mol^{-1} K^{-1}.

an increase in the population of unfolded molecules with decreased FRET efficiency due to the larger separation between the tryptophan donor and dansyl acceptor. The tryptophan fluorescence changes in a single-exponential phase with a time constant of 18 ± 5 μs at 303 K. In contrast, the dansyl fluorescence shows two distinct phases. The first has the same time constant (14 ± 5 μs) observed for tryptophan, while the slower phase, with a ~10 times greater amplitude, decays with a time constant of ~2 ms at 303 K. The fluorescence of the fast phase decreases, consistent with a decrease in the level of FRET corresponding to a net unfolding. The amplitude of the slow phase is also negative, and highly concentration dependent. At 0.25 mM, the slow phase disappears, while the relaxation time for the fast phase remains unchanged in both the dansyl and tryptophan fluorescence. These results suggest that the fast phase corresponds to the unfolding and refolding of the monomeric hairpin, while the slow phase is related to aggregation of the peptide.

To obtain the folding and unfolding rates, we fit the kinetic amplitudes and relaxation rates as a function of temperature with the following kinetic model:

$$3\mathrm{U} \underset{k_{-1}}{\overset{k_1}{\rightleftharpoons}} \mathrm{H_A} + \mathrm{H_B} + \mathrm{H_C} \underset{k_{-2}}{\overset{k_2}{\rightleftharpoons}} (\mathrm{H_AH_B}/3 + \mathrm{H_BH_C}/3 + \mathrm{H_CH_A}/3) + \mathrm{M} \underset{k_{-3}}{\overset{k_3}{\rightleftharpoons}} \mathrm{H_AH_BH_C}$$

where U is the unfolded monomeric peptide, H_A, H_B, and H_C are the three folded monomeric hairpins that make a trimer, H_AH_B, H_BH_C, and H_CH_A are the three possible dimers, M is $H_A/3 + H_B/3 + H_C/3$, and $H_AH_BH_C$ is the trimer of hairpins. For a homotrimer model, the three monomers and the three dimers are identical and are shown here only to illustrate the correct stoichiometry. The high-concentration data were fit because of its superior signal-to-noise ratio and also allowed the acquisition of kinetic information about the aggregation process. To simplify the kinetic analysis, all the rate equations were expressed in terms of monomer concentration and linearized for the two bimolecular processes, assuming that the temperature jump is a small perturbation of the equilibrium. This leads to a rate matrix that allows for easy optimization of the parameters in fitting the experimental relaxation times and amplitudes (see Materials and Methods). The populations of the four molecular species of the kinetic model resulting from the best fit are shown in Figure 7C, with the parameters of the kinetic model summarized in Table 1. In the fitting procedure, the dimer and trimer formation rate coefficients were constrained to be identical. The unfolded and folded monomer populations are equal at 354 K, consistent with the estimation of a T_m of >335 K obtained from the equilibrium thermal unfolding curve of Figure 3. The equilibrium constant at 298 K for the monomer ⇌ trimer equilibrium is 2.0×10^6 M^{-2}, which is in very good agreement with the sedimentation value of 1.1×10^6 M^{-2}. Table 2 compares the results at several temperatures. To fit the kinetic data with the minimum number of parameters, the activation heat capacities were not included, accounting for the larger differences observed at the extreme temperatures.

DISCUSSION

Both the NMR chemical shift data and NOEs indicate that this 17-residue peptide derived from the N-terminus of ubiquitin folds into a β-hairpin conformation (Figure 2). Moreover, the tryptophan and dansylated lysine modifications necessary to obtain a fluorescence signal for monitoring kinetics do not alter the conformation from that determined previously by Searle et al. (*90*). As frequently occurs with sequences that are found in β-hairpin conformations in proteins, this peptide aggregates. Careful sedimentation equilibrium studies show that at the concentrations used for kinetic studies, the aggregation is best described as a monomer ⇌ trimer equilibrium, with no detectable population of a dimer (Figure 4). Although the NMR lines broaden at the higher concentrations, the chemical shifts remain essentially unaltered, indicating that the assembled species is a trimer of β-hairpins.

The kinetic experiments reveal two phases: a concentration-independent relaxation at 15−20 μs, which we interpret as hairpin unfolding and refolding, and a concentration-dependent relaxation on the millisecond time scale, indicating an aggregation process (Figure 6). Motivated by the sedimentation equilibrium and NMR results, we modeled the aggregation process as a stepwise assembly of a trimer of hairpins. Both the relaxation rates and amplitudes (Figure 7) are readily explained by a kinetic model in which peptides unfolded into the hairpin structure in a simple two-state process and then assemble into unstable dimers and finally trimers (see Figure 7C). Because the kinetic amplitudes are determined by the populations, the kinetic model yields the folding and unfolding rate coefficients for the monomeric β-hairpin, as well as the monomer ⇌ trimer equilibrium constant. The good agreement between the equilibrium constants obtained from the sedimentation and kinetic data (Table 2) is an important test of the validity of the model.

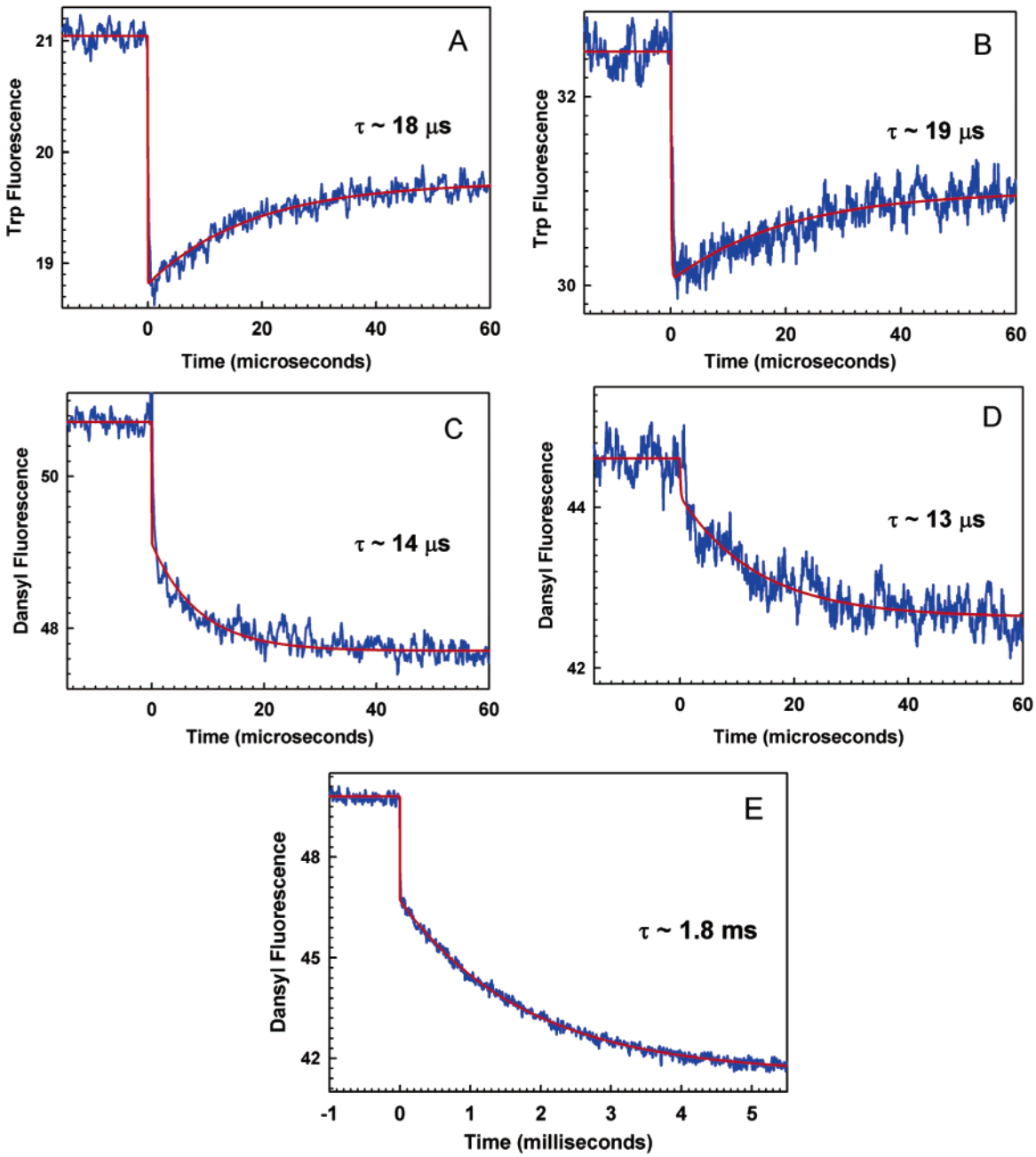

FIGURE 6: Kinetic progress curves at 303 K: (A) tryptophan fluorescence at 1.1 mM peptide, (B) tryptophan fluorescence at 0.2 mM peptide, (C) dansyl fluorescence at 1.1 mM peptide, (D) dansyl fluorescence at 0.2 mM peptide, and (E) dansyl fluorescence at 1.1 mM peptide. The temperature jump was ~10 K.

The kinetic model shows several interesting features. First, the slow and fast relaxations of the dansyl fluorescence, which differ by more than 100-fold, are completely uncoupled. This explains the concentration independence of the unfolding−refolding relaxation rate of the monomeric hairpin. The slow relaxation in the dansyl fluorescence is solely due to the dissociation and association of the trimer into folded monomers. The dimer and trimer association rates, which were constrained in the modeling to be the same, are 1.3×10^8 M^{-1} s^{-1}. The diffusion-limited rates for formation of the dimer and trimer calculated from the Smoluchowski equation for neutral species, i.e., $k = 4\pi(D_M + D_M)R$ and $k = 4\pi(D_M + D_D)R$, are 1.5×10^9 and 1.3×10^9 M^{-1} s^{-1}, where R is the critical radius assumed to be 0.4 nm and the diffusion coefficients, D_M and D_D for the monomer and dimer, respectively, are calculated from the empirical equation given by Lapidus et al. (*97*). However, there is a net charge, z_M, of −1 on the monomer and a z_D of −2 on the dimer, so electrostatic repulsion will reduce these rates somewhat. We can estimate this reduction from the Debye−Smoluchowski equation (*98*):

$$k_{D-S} = 4\pi(D_M + D_D)\frac{z_M z_D e^2/\epsilon k_B T}{\exp(z_M z_D e^2/R\epsilon k_B T) - 1} \times \exp(2.3 z_M z_D I^{1/2}) \quad (6)$$

where the second factor accounts for the electrostatic repulsion and the third factor for the ionic screening arising from the 50 mM sodium bicarbonate buffer at pH 10.5 with an ionic strength (I) of 0.1 (e is the charge on an electron and ϵ is the dielectric constant of water). The calculated rates

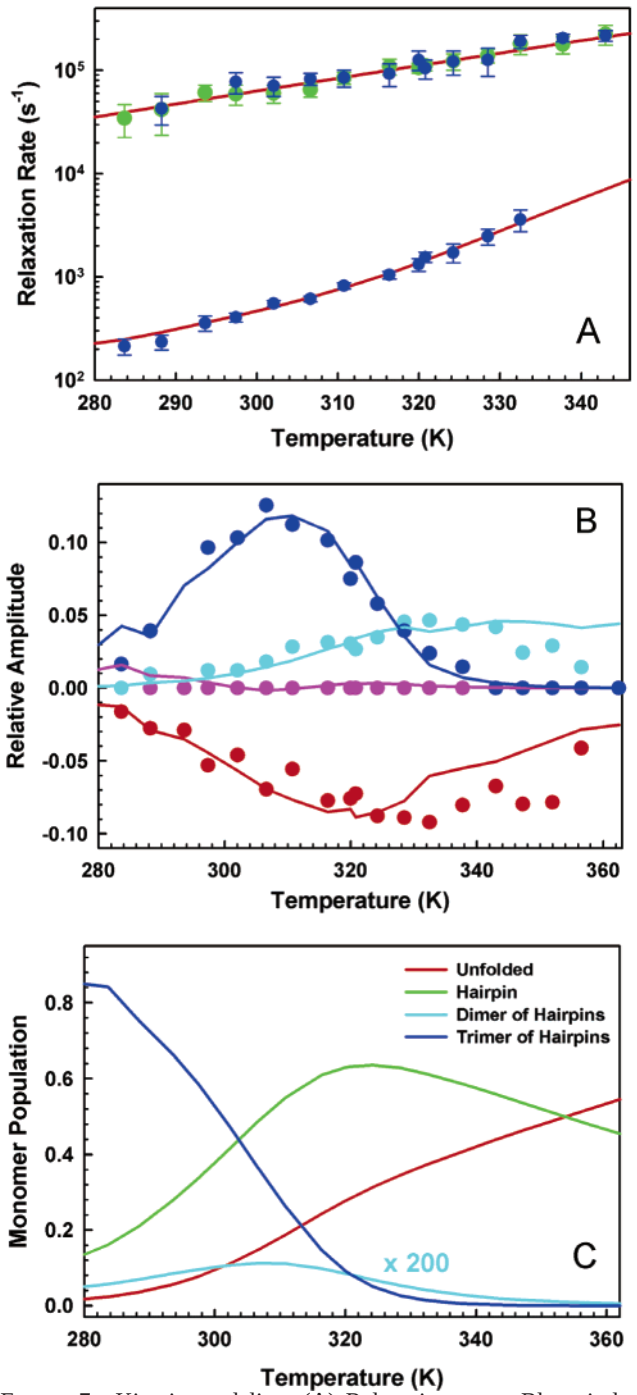

FIGURE 7: Kinetic modeling. (A) Relaxation rates. Blue circles correspond to the rates determined from dansyl fluorescence, and green circles correspond to the rates determined from tryptophan fluorescence. The continuous red lines correspond to the results from the fit. (B) Relative kinetic amplitudes calculated as the change in fluorescence due to each kinetic phase divided by the equilibrium value of fluorescence at the initial temperature. Circles correspond to the experimental values and continuous lines to the results from the fit: (red) tryptophan fluorescence fast phase, (cyan) dansyl fluorescence fast phase, (magenta) tryptophan fluorescence slow phase, and (blue) dansyl fluorescence slow phase. (C) Populations of peptide molecules in each of the fours species of the kinetic model at a total concentration of 1.1 mM: (red line) unfolded, (green line) monomeric hairpin, (cyan line) population of the dimer of hairpins multiplied by a factor of 200 to allow visual inspection, and (blue line) trimer of hairpins. The concentration of trimer (dimer) is obtained by dividing the value in the plot by 3 (2).

at 298 K are 1.1×10^9 and 6×10^8 M^{-1} s^{-1} for dimer and trimer association, respectively. The observed rate of 1.3×10^8 M^{-1} s^{-1} is therefore not far from diffusion-limited rate, indicating that there is a very small free energy barrier to association once an encounter complex is formed. This result suggests that there is very little structural reorganization associated with oligomerization, consistent with our conclusion from the NMR results in which the structure of the individual hairpins in the trimer is very similar to that of the monomer.

Table 2: Comparison of Monomer ⇌ Trimer Equilibrium Constants Determined from Kinetic Modeling of Relaxation Rates and Amplitudes and from Sedimentation Equilibrium Experiments[a]

T (K)	$K_{1,3}$ (kinetics)[b] (M^{-2})	$K_{1,3}$ (sedimentation)[c] (M^{-2})
293	5.4×10^6	1.3×10^6
298	2.0×10^6	1.1×10^6
303	7.8×10^5	7.5×10^5
313	1.2×10^5	2.9×10^5
323	2.0×10^4	8.1×10^4
333	3.5×10^3	1.7×10^4
343	0.7×10^3	2.9×10^3

[a] The equilibrium constant is defined as [trimer]/[monomer]^3, where the monomer concentration is the sum of the folded and unfolded monomeric peptide concentrations. [b] Calculated from the populations generated by the kinetic model given in Figure 7C, assuming zero activation heat capacities. [c] Calculated from eq 2 with the following thermodynamic parameters: $T_0 = 298$ K, $\Delta H_0 = -10.4$ kcal/mol, $\Delta S_0 = -7.3$ cal mol^{-1} K^{-1}, and $\Delta C_p = -760$ cal mol^{-1} K^{-1}.

The folding time for the monomeric hairpin of 17 μs calculated from the model is associated with an activation energy of only 4 kcal/mol (Table 1). By using viscogens that affected neither the equilibrium constants nor the activation energy, Jas et al. showed that the folding time for the GB1 hairpin scales inversely with the first power of the solvent viscosity, as predicted from Kramers theory in the high-friction limit (*84*, *99*). The change in water viscosity with temperature contributes ~4 kcal/mol to the observed activation energy. Assuming that the viscosity dependence is the same for the hairpin studied here and the GB1 hairpin, the intrinsic activation energy for hairpin formation is therefore essentially zero, as also found for the GB1 hairpin. In the case of the GB1 hairpin, the near-zero apparent activation energy was explained by an Ising-like model discussed below (*2*, *5*). The free energy versus native peptide bond surface calculated from the partition function showed that the structures at the free energy maximum are lower in energy than the structures of the unfolded state.[1] This explanation could also apply to the present hairpin for both the folding of the monomeric hairpin and the assembly reaction. In the case of the assembly reaction, the value of −3 kcal/mol (Table 1) (with an intrinsic activation energy of −7 kcal/mol after correction for the viscosity effect) indicates stabilizing interactions between individual hairpins in the transition state for the process of association from an encounter complex.

[1] On the basis of a simulation study, Dinner and Karplus argued that the presence of a free energy barrier in the model of Muñoz et al. (*2*, *5*) results from their single-sequence approximation that only one single stretch of native residues is allowed in each molecule (*13*). However, the conclusion of Dinner and Karplus has been shown to be incorrect, since evaluation of the partition function without any restriction on the number of native stretches (i.e., all $2^N = 32\,768$ species) also exhibits a free energy profile with a significant barrier as well as only two minima (E. R. Henry and W. A. Eaton, unpublished results) (*8*, *51*), thereby explaining the two-state behavior observed experimentally by Muñoz et al. (*2*) and Honda et al. (*3*).

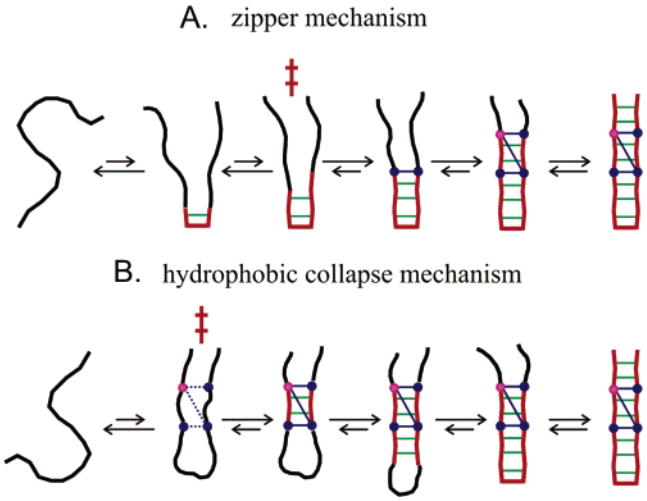

FIGURE 8: Schematic pictures of the zipper and hydrophobic collapse mechanism. (A) Zipper mechanism. In this mechanism, structure formation is initiated at the turn. The description of this mechanism can be made quantitative with the Ising-like model of Muñoz et al. (see the text for description) (*2*, *5*). This model shows that the stabilization from forming cross-strand hydrogen bonds (green bars) is insufficient to overcome the entropy loss of ordering peptide bonds (and side chains) into their native conformation. The blue bars represent van der Waals interactions between hydrophobic residues. The free energy barrier is crossed once the first hydrophobic contact is made (see Figure 9). (B) Hydrophobic collapse mechanism. In this mechanism, a disordered loop forms that brings the hydrophobic cluster together with the formation of partial formation of the hydrophobic interactions present in the final native cluster, indicated by the dotted blue line. The free energy barrier is crossed once the full stabilization is realized from the fully native hydrophobic cluster.

The most important information to be derived from the kinetics is insight into the mechanism of β-hairpin formation. For the sake of discussion, it is useful to consider two rather different mechanisms that have been extensively discussed for the GB1 hairpin: one in which structure formation is initiated at the turn and another in which the hydrophobic cluster forms first. For a lack of better names, we refer to these as the zipper and hydrophobic collapse mechanisms, respectively. In the zipper mechanism, turn formation is followed by propagation of structure toward the amino and carboxy termini with sequential formation of cross-strand hydrogen bonds and the hydrophobic cluster (Figure 8). In the hydrophobic collapse mechanism, cluster formation is followed by propagation of structure outward in both directions to form hydrogen bonds and the turn.

A quantitative analysis of the zipper model can be made with the Ising-like model of Muñoz et al. (*2*, *5*). In this model, which ignores non-native interactions, residues exist in either native or non-native conformations and no contacts can be made unless all intervening residues are in their native

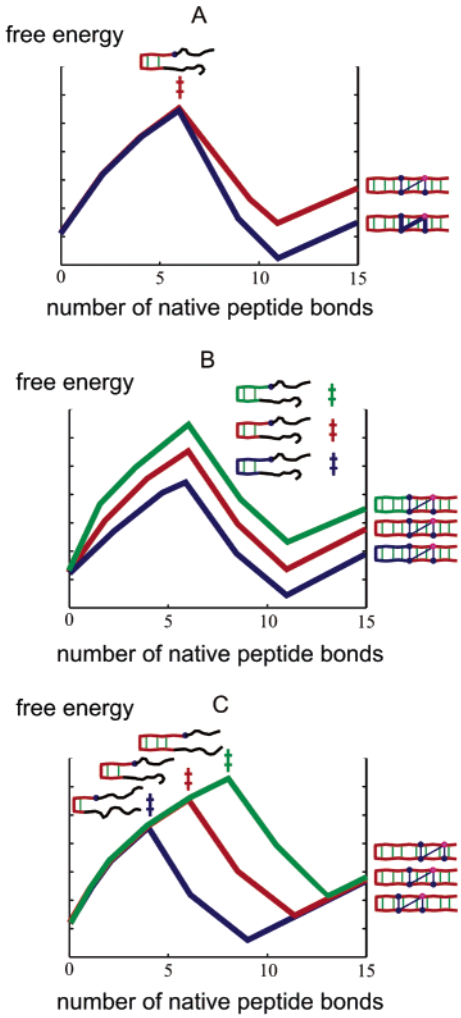

FIGURE 9: Predictions of the zipper mechanism. (A) Increasing the stability of the hydrophobic cluster, indicated by the thicker blue bars, stabilizes the hairpin but does not change the folding rate. (B) Increasing (blue) or decreasing (green) the turn propensity can be viewed as decreasing or increasing the entropy cost of forming the turn, respectively, which would lower the free energy barrier and stabilize the folded structure. (C) Moving the cluster closer to the turn would require fewer residues to be ordered before the stabilization from the hydrophobic cluster would be realized and, therefore, a smaller entropy cost to reach the transition state.

conformation.[2] Only two thermodynamic factors are considered: the stabilizing interactions from side chain interactions and cross-strand hydrogen bonds and the destabilizing entropy cost of ordering residues in their native conformation. The free energy profiles generated from the partition function of the model show that the folding barrier is not crossed until the first hydrophobic contact is formed, the stabilizing energy of the first two cross-strand hydrogen bonds alone being insufficient to compensate for the entropy loss associated with ordering residues in their native conformation (Figure 9).

The model of Muñoz et al. makes several predictions that can be used to test a zipper mechanism, as shown in Figure 9. First, amino acid replacements that stabilize the hydrophobic cluster should have little or no effect on the folding rate (Figure 9A). Second, decreasing the entropic cost of forming the turn should increase the folding rate (Figure 9B). Finally, moving the stabilizing cluster farther from the turn should increase the free energy barrier because of the

[2] This latter assumption of the model rules out the possibility of first connecting the cluster with a disordered loop. Muñoz et al. assumed that forming a seven-residue loop would require ~1 μs, comparable to the hairpin formation time of 6 μs, so they could not rule out simple collapse with a disordered loop connecting the residues of the hydrophobic cluster as being rate-limiting (*2*). They chose to develop a model that enforces a "zipper" mechanism since it yields a more straightforward set of kinetic equations for fitting the experimental data. We now know from several subsequent studies that the time required to form a disordered loop of 5−10 residues is on the order of 0.1 μs (*97*, *100*−*107*), so disordered loop formation cannot be rate-limiting.

Table 3: Folding Times of β-Hairpins

name or source	sequence	folding time (μs)	stability (kcal/mol)	T (K)	ref
ubiquitin-based peptide	MQIWVKNPDGTITLEVK	21	−0.9	298	this work
GB1	GEWTYDDATKTFTVTE	6.0[a]	0[a]	297	*2*
			0.2[b]	298	*3*
			0.1[c]	298	*3*
		18[d]	0.7[d]	298	*89*
(D7P)-GB1	GEWTYDPATKTFTVTE	17	−0.5	298	*89*
GB1m2	GEWTYNPATGKFTVTE	5	−0.4	298	*89*
GB1m2	GEWTYNPATGKFTVTE	2	−0.8	298	*89*
trpzip1	SWTWEGNKWTWK	6.3	−0.6	296	*87*
trpzip2	SWTWENGKWTWK	2.5	0	296	*87*
trpzip3	SWTWE^{D}PNKWTWK	1.7	−1.2	296	*87*
trpzip3-1	SWTWDATKWTWK	52	−0.2	296	*87*
trpzip4	GEWTWDDATKTWTWTE	15	−1.6	297	*87*
		15	−1.6	298	*89*
peptide I	SESYINPDGTWTVTE	0.8	ca. −1	303	*85*
MrH3a	KKYTVSINGKKITVSA	4.7	0	323	*86*
BH8[e]	EGITVNGKTYGR	1.1	0	298	*86*

[a] From fluorescence. [b] From NMR. [c] From calorimetry. [d] From NMR. [e] Measured in 21% hexafluoro-2-propanol.

additional entropic cost of ordering more residues to reach the barrier top, while decreasing this distance should decrease the barrier (Figure 9C) (this, in fact, is the simplest explanation of the correlation between contact order and folding rates) (*48*, *51*, *108*).

The "hydrophobic collapse" mechanism has not yet been formulated in terms of a quantitative model. A pictorial representation of this mechanism (Figure 9) reveals that a detailed description is more subtle than for the zipper model. The clearest prediction of the hydrophobic collapse mechanism is that the folding rate should not depend on the residues in the turn region, since disordered loops for a wide range of sequences form much faster than a hairpin and with very similar rates (*97*, *100*−*106*, *109*, *110*). Assuming that the cluster is partially formed in the transition state, this model predicts that the hairpin formation rate is faster for more stable clusters.

Table 3 shows the folding times for the 13 β-hairpins that have been studied up to now. The range of folding times is rather narrow, varying from 0.8 to 52 μs, corresponding to only 2.5 kcal/mol in activation free energy and making it somewhat risky to draw firm conclusions by comparing the rates for the different peptides. Nevertheless, the results and analysis of the careful study of Gai and co-workers are enlightening (*87*). They found that trpzip4, which has the same turn sequence as GB1, folds with half the rate even though it is 15-fold more stable, consistent with the first prediction of the model of Muñoz et al. for a zipper mechanism (*87*) (Figure 9A) and inconsistent with a hydrophobic collapse mechanism. Gai and co-workers also found an excellent correlation between the folding times and equilibrium entropy cost for the four 12-residue trpzip peptides (Table 2) (*87*), which differ only in turn sequences. If the differences are due to differences in entropy required to reach the barrier top, then this correlation is consistent with the second prediction of the zipper model (*87*) (Figure 9B) but inconsistent with the hydrophobic collapse model that predicts no effect of the intervening sequence between the hydrophobic residues of the cluster.

These results do not allow a rigorous test of the third prediction of the zipper model, the effect of repositioning of the stabilizing hydrophobic contact on the folding rate. However, it is interesting to note that the ubiquitin peptide studied here has the same turn sequence and approximately the same stability as peptide I but folds ∼25 times more slowly (Table 2). The zipper model provides a simple explanation. Assuming that the free energy barrier is crossed after the first interaction is made between hydrophobic residues (W-L in the ubiquitin peptide and W-I in peptide I, Table 2), eight residues must first be ordered in the ubiquitin peptide to reach the barrier top, and this is associated with the formation of two hydrogen bonds; for peptide I, the corresponding numbers are four residues and one hydrogen bond. Using the entropy cost of 2.7 cal mol^{-1} K^{-1} and 1.0 kcal/mol per hydrogen bond from the data fitting of Muñoz et al. (*5*), the ubiquitin peptide is predicted to fold ∼50 times more slowly, in surprisingly good agreement with experiment.

Both experiments and analytical models can provide insights into mechanism but cannot provide the wealth of detail and information about mechanism that can be extracted from simulations. Multiple folding trajectories using all-atom molecular dynamics simulations in explicit solvent contain, in principle, everything that one can learn about the folding mechanism. Although such calculations have not yet been performed, a wide range of approximate simulation methods have been employed to study the β-hairpin from protein GB1 (*10*−*47*). The majority have favored a mechanism similar to the hydrophobic collapse mechanism (Figure 8) (*10*, *13*−*18*, *20*, *25*, *30*, *31*, *36*, *44*, *111*). However, other simulation studies suggest a zipper mechanism (*12*, *21*), simultaneous zipping and collapse (*19*, *34*), or a mechanism more complicated than either (*27*, *33*, *40*), such as the initial formation of an α-helix (*43*). The mechanisms presumably differ because of different force fields and different simulation techniques, e.g., direct observation from trajectories or mechanisms inferred from free energy surfaces. Swope and Pitera have made the interesting suggestion that the diversity of mechanisms may also arise from different criteria for the existence of hydrogen bonds (*35*). Depending on the criteria, they find either zipper or hydrophobic collapse mechanisms.

A major deficiency in the simulation studies is that, with just a few exceptions, there has been little or no quantitative comparison with experimental data. The data for the GB1 hairpin include thermal unfolding curves measured from the tryptophan fluorescence quantum yields (*2*), from Förster

resonance energy transfer between the tryptophan and dansylated lysine (which also gives information about the inter-residue distance in the unfolded state) (*2*), from NMR chemical shifts (*3*, *89*), and from calorimetry (*3*), and relaxation rates as a function of temperature determined directly by fluorescence (*2*) or indirectly by NMR line broadening (*89*). There are only a few calculations that come close to accurately reproducing experimental unfolding curves (*47*) or rates (*30*, *31*, *44*) and only one that has reproduced both, albeit in a simplified representation of the peptide structure (*14*). Until a closer connection is made between simulations and experiments, it will not be possible to take advantage of the enormous amount of detail contained in the simulations to unravel the folding mechanism or mechanisms of β-hairpins.

REFERENCES

1. Blanco, F. J., Rivas, G., and Serrano, L. (1994) A short linear peptide that folds into a β-hairpin in aqueous solution, *Nat. Struct. Biol. 1*, 584−590.
2. Muñoz, V., Thompson, P. A., Hofrichter, J., and Eaton, W. A. (1997) Folding dynamics and mechanism of β-hairpin formation, *Nature 390*, 196−199.
3. Honda, S., Kobayashi, N., and Munekata, E. (2000) Thermodynamics of a β-hairpin structure: Evidence for cooperative formation of folding nucleus, *J. Mol. Biol. 295*, 269−278.
4. Kobayashi, N., Honda, S., Yoshii, H., and Munekata, E. (2000) Role of side-chains in the cooperative β-hairpin folding of the short C-terminal fragment derived from streptococcal protein G, *Biochemistry 39*, 6564−6571.
5. Muñoz, V., Henry, E. R., Hofrichter, J., and Eaton, W. A. (1998) A statistical mechanical model for β-hairpin kinetics, *Proc. Natl. Acad. Sci. U.S.A. 95*, 5872−5879.
6. Guo, C. L., Levine, H., and Kessler, D. A. (2000) How does a β-hairpin fold/unfold? Competition between topology and heterogeneity in a solvable model, *Proc. Natl. Acad. Sci. U.S.A. 97*, 10775−10779.
7. Guo, C. L., Levine, H., and Kessler, D. A. (2000) Two state behavior in a solvable model of β-hairpin folding, *Phys. Rev. Lett. 84*, 3490−3493.
8. Bruscolini, P., and Pelizzola, A. (2002) Exact solution of the Munoz-Eaton model for protein folding, *Phys. Rev. Lett. 88*, 258101-1−258101-4.
9. Bruscolini, P., and Cecconi, F. (2003) Mean-field approach for a statistical mechanical model of proteins, *J. Chem. Phys. 119*, 1248−1256.
10. Pande, V. S., and Rokhsar, D. S. (1999) Molecular dynamics simulations of unfolding and refolding of a β-hairpin fragment of protein G, *Proc. Natl. Acad. Sci. U.S.A. 96*, 9062−9067.
11. Roccatano, D., Amadei, A., Di Nola, A., and Berendsen, H. J. C. (1999) A molecular dynamics study of the 41−56 β-hairpin from B1 domain of protein G, *Protein Sci. 8*, 2130−2143.
12. Kolinski, A., Ilkowski, B., and Skolnick, J. (1999) Dynamics and thermodynamics of β-hairpin assembly: Insights from various simulation techniques, *Biophys. J. 77*, 2942−2952.
13. Dinner, A. R., Lazaridis, T., and Karplus, M. (1999) Understanding β-hairpin formation, *Proc. Natl. Acad. Sci. U.S.A. 96*, 9068−9073.
14. Klimov, D. K., and Thirumalai, D. (2000) Mechanisms and kinetics of β-hairpin formation, *Proc. Natl. Acad. Sci. U.S.A. 97*, 2544−2549.
15. Ma, B. Y., and Nussinov, R. (2000) Molecular dynamics simulations of a β-hairpin fragment of protein G: Balance between side-chain and backbone forces, *J. Mol. Biol. 296*, 1091−1104.
16. Bryant, Z., Pande, V. S., and Rokhsar, D. S. (2000) Mechanical unfolding of a β-hairpin using molecular dynamics, *Biophys. J. 78*, 584−589.
17. Lee, J., and Shin, S. M. (2001) Understanding β-hairpin formation by molecular dynamics simulations of unfolding, *Biophys. J. 81*, 2507−2516.
18. Garcia, A. E., and Sanbonmatsu, K. Y. (2001) Exploring the energy landscape of a β hairpin in explicit solvent, *Proteins 42*, 345−354.
19. Zhou, R. H., Berne, B. J., and Germain, R. (2001) The free energy landscape for β hairpin folding in explicit water, *Proc. Natl. Acad. Sci. U.S.A. 98*, 14931−14936.
20. Eastman, P., Gronbech-Jensen, N., and Doniach, S. (2001) Simulation of protein folding by reaction path annealing, *J. Chem. Phys. 114*, 3823−3841.
21. Tsai, J., and Levitt, M. (2002) Evidence of turn and salt bridge contributions to β-hairpin stability: MD simulations of C-terminal fragment from the B1 domain of protein G, *Biophys. Chem. 101*, 187−201.
22. Jang, S., Shin, S., and Pak, Y. (2002) Molecular dynamics study of peptides in implicit water: Ab initio folding of β-hairpin, β-sheet, and ββα-motif, *J. Am. Chem. Soc. 124*, 4976−4977.
23. Cieplak, M., Hoang, T. X., and Robbins, M. O. (2002) Thermal folding and mechanical unfolding pathways of protein secondary structures, *Proteins 49*, 104−113.
24. Zhou, R. H., and Berne, B. J. (2002) Can a continuum solvent model reproduce the free energy landscape of a β-hairpin folding in water? *Proc. Natl. Acad. Sci. U.S.A. 99*, 12777−12782.
25. Lee, J., and Shin, S. (2002) Two-dimensional correlation analysis of peptide unfolding: Molecular dynamics simulations of β hairpins, *J. Phys. Chem. B 106*, 8796−8802.
26. Klimov, D. K., Newfield, D., and Thirumalai, D. (2002) Simulations of β-hairpin folding confined to spherical pores using distributed computing, *Proc. Natl. Acad. Sci. U.S.A. 99*, 8019−8024.
27. Wei, G. H., Derreumaux, P., and Mousseau, N. (2003) Sampling the complex energy landscape of a simple β-hairpin, *J. Chem. Phys. 119*, 6403−6406.
28. Ma, B. Y., and Nussinov, R. (2003) Energy landscape and dynamics of the β-hairpin G peptide and its isomers: Topology and sequences, *Protein Sci. 12*, 1882−1893.
29. Zhou, R. H. (2003) Free energy landscape of protein folding in water: Explicit vs. implicit solvent, *Proteins 53*, 148−161.
30. Bolhuis, P. G. (2003) Transition-path sampling of β-hairpin folding, *Proc. Natl. Acad. Sci. U.S.A. 100*, 12129−12134.
31. Pande, V. S., Baker, I., Chapman, J., Elmer, S. P., Khaliq, S., Larson, S. M., Rhee, Y. M., Shirts, M. R., Snow, C. D., Sorin, E. J., and Zagrovic, B. (2003) Atomistic protein folding simulations on the submillisecond time scale using worldwide distributed computing, *Biopolymers 68*, 91−109.
32. Zhou, Y. Q., Zhang, C., Stell, G., and Wang, J. (2003) Temperature dependence of the distribution of the first passage time: Results from discontinuous molecular dynamics simulations of an all-atom model of the second β-hairpin fragment of protein G, *J. Am. Chem. Soc. 125*, 6300−6305.
33. Evans, D. A., and Wales, D. J. (2004) Folding of the GB1 hairpin peptide from discrete path sampling, *J. Chem. Phys. 121*, 1080−1090.
34. Felts, A. K., Harano, Y., Gallicchio, E., and Levy, R. M. (2004) Free energy surfaces of β-hairpin and α-helical peptides generated by replica exchange molecular dynamics with the AGBNP implicit solvent model, *Proteins 56*, 310−321.
35. Swope, W. C., Pitera, J. W., Suits, F., Pitman, M., Eleftheriou, M., Fitch, B. G., Germain, R. S., Rayshubski, A., Ward, T. J. C., Zhestkov, Y., and Zhou, R. (2004) Describing protein folding kinetics by molecular dynamics simulations. 2. Example applications to alanine dipeptide and β-hairpin peptide, *J. Phys. Chem. B 108*, 6582−6594.
36. Krivov, S. V., and Karplus, M. (2004) Hidden complexity of free energy surfaces for peptide (protein) folding, *Proc. Natl. Acad. Sci. U.S.A. 101*, 14766−14770.
37. Paschek, D., and Garcia, A. E. (2004) Reversible temperature and pressure denaturation of a protein fragment: A replica exchange molecular dynamics simulation study, *Phys. Rev. Lett. 93*, 238105-1−238105-4.
38. Irback, A., and Sjunnesson, F. (2004) Folding thermodynamics of three β-sheet peptides: A model study, *Proteins 56*, 110−116.
39. Yoda, T., Sugita, Y., and Okamoto, Y. (2004) Secondary-structure preferences of force fields for proteins evaluated by generalized-ensemble simulations, *Chem. Phys. 307*, 269−283.
40. Lee, I. H., Kim, S. Y., and Lee, J. (2005) Dynamic folding pathway models of α-helix and β-hairpin structures, *Chem. Phys. Lett. 412*, 307−312.
41. Carr, J. M., Trygubenko, S. A., and Wales, D. J. (2005) Finding pathways between distant local minima, *J. Chem. Phys. 122*, 234903.

42. Irback, A. (2005) Peptide folding and aggregation studied using a simplified atomic model, *J. Phys.: Condens. Matter 17*, S1553−S1564.
43. Andrec, M., Felts, A. K., Gallicchio, E., and Levy, R. M. (2005) Protein folding pathways from replica exchange simulations and a kinetic network model, *Proc. Natl. Acad. Sci. U.S.A. 102*, 6801−6806.
44. Bolhuis, P. G. (2005) Kinetic pathways of β-hairpin (Un)folding in explicit solvent, *Biophys. J. 88*, 50−61.
45. Gallicchio, E., Andrec, M., Felts, A. K., and Levy, R. M. (2005) Temperature weighted histogram analysis method, replica exchange, and transition paths, *J. Phys. Chem. B 109*, 6722−6731.
46. Zhu, J., Alexov, E., and Honig, B. (2005) Comparative study of generalized Born models: Born radii and peptide folding, *J. Phys. Chem. B 109*, 3008−3022.
47. Irback, A., and Mohanty, S. (2005) Folding thermodynamics of peptides, *Biophys. J. 88*, 1560−1569.
48. Muñoz, V., and Eaton, W. A. (1999) A simple model for calculating the kinetics of protein folding from three-dimensional structures, *Proc. Natl. Acad. Sci. U.S.A. 96*, 11311−11316.
49. Ivankov, D. N., and Finkelstein, A. V. (2001) Theoretical study of a landscape of protein folding−unfolding pathways. Folding rates at midtransition, *Biochemistry 40*, 9957−9961.
50. Alm, E., Morozov, A. V., Kortemme, T., and Baker, D. (2002) Simple physical models connect theory and experiment in protein folding kinetics, *J. Mol. Biol. 322*, 463−476.
51. Henry, E. R., and Eaton, W. A. (2004) Combinatorial modeling of protein folding kinetics: Free energy profiles and rates, *Chem. Phys. 307*, 163−185.
52. De Alba, E., Rico, M., and Jimenez, M. A. (1999) The turn sequence directs β-strand alignment in designed β-hairpins, *Protein Sci. 8*, 2234−2244.
53. Syud, F. A., Espinosa, J. F., and Gellman, S. H. (1999) NMR-based quantification of β-sheet populations in aqueous solution through use of reference peptides for the folded and unfolded states, *J. Am. Chem. Soc. 121*, 11577−11578.
54. Searle, M. S., Griffiths-Jones, S. R., and Skinner-Smith, H. (1999) Energetics of weak interactions in a β-hairpin peptide: Electrostatic and hydrophobic contributions to stability from lysine salt bridges, *J. Am. Chem. Soc. 121*, 11615−11620.
55. Odaert, B., Jean, F., Boutillon, C., Buisine, E., Melnyk, O., Tartar, A., and Lippens, G. (1999) Synthesis, folding, and structure of the β-turn mimic modified B1 domain of streptococcal protein G, *Protein Sci. 8*, 2773−2783.
56. Griffiths-Jones, S. R., Maynard, A. J., and Searle, M. S. (1999) Dissecting the stability of a β-hairpin peptide that folds in water: NMR and molecular dynamics analysis of the β-turn and β-strand contributions to folding, *J. Mol. Biol. 292*, 1051−1069.
57. Santiveri, C. M., Rico, M., and Jimenez, M. A. (2000) Position effect of cross-strand side-chain interactions on β-hairpin formation, *Protein Sci. 9*, 2151−2160.
58. Stanger, H. E., Syud, F. A., Espinosa, J. F., Giriatt, I., Muir, T., and Gellman, S. H. (2001) Length-dependent stability and strand length limits in antiparallel β-sheet secondary structure, *Proc. Natl. Acad. Sci. U.S.A. 98*, 12015−12020.
59. Espinosa, J. F., Muñoz, V., and Gellman, S. H. (2001) Interplay between hydrophobic cluster and loop propensity in β-hairpin formation, *J. Mol. Biol. 306*, 397−402.
60. Cochran, A. G., Skelton, N. J., and Starovasnik, M. A. (2001) Tryptophan zippers: Stable, monomeric β-hairpins, *Proc. Natl. Acad. Sci. U.S.A. 98*, 5578−5583.
61. Espinosa, J. F., Syud, F. A., and Gellman, S. H. (2002) Analysis of the factors that stabilize a designed two-stranded antiparallel β-sheet, *Protein Sci. 11*, 1492−1505.
62. Gibbs, A. C., Bjorndahl, T. C., Hodges, R. S., and Wishart, D. S. (2002) Probing the structural determinants of type II′ β-turn formation in peptides and proteins, *J. Am. Chem. Soc. 124*, 1203−1213.
63. Santiveri, C. M., Santoro, J., Rico, M., and Jimenez, M. A. (2002) Thermodynamic analysis of β-hairpin-forming peptides from the thermal dependence of H-1 NMR chemical shifts, *J. Am. Chem. Soc. 124*, 14903−14909.
64. Hilario, J., Kubelka, J., and Keiderling, T. A. (2003) Optical spectroscopic investigations of model β-sheet hairpins in aqueous solution, *J. Am. Chem. Soc. 125*, 7562−7574.
65. Blandl, T., Cochran, A. G., and Skelton, N. J. (2003) Turn stability in β-hairpin peptides: Investigation of peptides containing 3:5 type I G1 bulge turns, *Protein Sci. 12*, 237−247.
66. Ciani, B., Jourdan, M., and Searle, M. S. (2003) Stabilization of β-hairpin peptides by salt bridges: Role of preorganization in the energetic contribution of weak interactions, *J. Am. Chem. Soc. 125*, 9038−9047.
67. Searle, M. S. (2004) Insights into stabilizing weak interactions in designed peptide β-hairpins, *Biopolymers 76*, 185−195.
68. Wang, T., Xu, Y., Du, D. G., and Gai, F. (2004) Determining β-sheet stability by Fourier transform infrared difference spectra, *Biopolymers 75*, 163−172.
69. Fesinmeyer, R. M., Hudson, F. M., and Andersen, N. H. (2004) Enhanced hairpin stability through loop design: The case of the protein G B1 domain hairpin, *J. Am. Chem. Soc. 126*, 7238−7243.
70. Ahmed, Z., Beta, I. A., Mikhonin, A. V., and Asher, S. A. (2005) UV-resonance Raman thermal unfolding study of Trp-cage shows that it is not a simple two-state miniprotein, *J. Am. Chem. Soc. 127*, 10943−10950.
71. Wang, H. W., and Sung, S. S. (1999) Effects of turn residues on β-hairpin folding: A molecular dynamics study, *Biopolymers 50*, 763−776.
72. Galzitskaya, O. V., Higo, J., Kuroda, M., and Nakamura, H. (2000) β-Hairpin folds by molecular dynamics simulations, *Chem. Phys. Lett. 326*, 421−429.
73. Ferrara, P., Apostolakis, J., and Caflisch, A. (2000) Thermodynamics and kinetics of folding of two model peptides investigated by molecular dynamics simulations, *J. Phys. Chem. B 104*, 5000−5010.
74. Bonvin, A., and van Gunsteren, W. F. (2000) β-Hairpin stability and folding: Molecular dynamics studies of the first β-hairpin of Tendamistat, *J. Mol. Biol. 296*, 255−268.
75. Kamiya, N., Higo, J., and Nakamura, H. (2002) Conformational transition states of a β-hairpin peptide between the ordered and disordered conformations in explicit water, *Protein Sci. 11*, 2297−2307.
76. Wu, H. W., Wang, S. M., and Brooks, B. R. (2002) Direct observation of the folding and unfolding of a β-hairpin in explicit water through computer simulation, *J. Am. Chem. Soc. 124*, 5282−5283.
77. Lei, H. X., and Smith, P. E. (2003) The role of the unfolded state in hairpin stability, *Biophys. J. 85*, 3513−3520.
78. Gnanakaran, S., and Garcia, A. E. (2003) Folding of a highly conserved diverging turn motif from the SH3 domain, *Biophys. J. 84*, 1548−1562.
79. Santiveri, C. M., Jimenez, M. A., Rico, M., Van Gunsteren, W. F., and Daura, X. (2004) β-Hairpin folding and stability: Molecular dynamics simulations of designed peptides in aqueous solutions, *J. Pept. Sci. 10*, 546−565.
80. Wu, X. W., and Brooks, B. R. (2004) β-Hairpin folding mechanism of a nine-residue peptide revealed from molecular dynamics simulations in explicit water, *Biophys. J. 86*, 1946−1958.
81. Ulmschneider, J. P., and Jorgensen, W. L. (2004) Polypeptide folding using Monte Carlo sampling, concerted rotation, and continuum solvation, *J. Am. Chem. Soc. 126*, 1849−1857.
82. Yang, W. Y., Pitera, J. W., Swope, W. C., and Gruebele, M. (2004) Heterogeneous folding of the trpzip hairpin: Full atom simulation and experiment, *J. Mol. Biol. 336*, 241−251.
83. Higo, J., Galzitskaya, O. V., Ono, S., and Nakamura, H. (2001) Energy landscape of a β-hairpin peptide in explicit water studied by multicanonical molecular dynamics, *Chem. Phys. Lett. 337*, 169−175.
84. Jas, G. S., Eaton, W. A., and Hofrichter, J. (2001) Effect of viscosity on the kinetics of α-helix and β-hairpin formation, *J. Phys. Chem. B 105*, 261−272.
85. Xu, Y., Oyola, R., and Gai, F. (2003) Infrared study of the stability and folding kinetics of a 15-residue β-hairpin, *J. Am. Chem. Soc. 125*, 15388−15394.
86. Dyer, R. B., Maness, S. J., Peterson, E. S., Franzen, S., Fesinmeyer, R. M., and Andersen, N. H. (2004) The mechanism of β-hairpin formation, *Biochemistry 43*, 11560−11566.
87. Du, D. G., Zhu, Y. J., Huang, C. Y., and Gai, F. (2004) Understanding the key factors that control the rate of β-hairpin folding, *Proc. Natl. Acad. Sci. U.S.A. 101*, 15915−15920.
88. Dyer, R. B., Maness, S. J., Franzen, S., Fesinmeyer, R. M., Olsen, K. A., and Andersen, N. H. (2005) Hairpin folding dynamics: The cold-denatured state is predisposed for rapid refolding, *Biochemistry 44*, 10406−10415.
89. Olsen, K. A., Fesinmeyer, R. M., Stewart, J. M., and Andersen, N. H. (2005) Hairpin folding rates reflect mutations within and

remote from the turn region, *Proc. Natl. Acad. Sci. U.S.A. 102*, 15483−15487.
90. Searle, M. S., Williams, D. H., and Packman, L. C. (1995) A short linear peptide derived from the N-terminal sequence of ubiquitin folds into a water-stable non-native β-hairpin, *Nat. Struct. Biol. 2*, 999−1006.
91. Ghirlando, R., Keown, M. B., MacKay, G., Lewis, M. S., Unkeless, J. C., and Gould, H. J. (1995) Stoichiometry and thermodynamics of the interaction between the Fc fragment of human IgG_1 and its low-affinity receptor FcγRIII, *Biochemistry 34*, 13320−3327.
92. Roark, D. E. (1976) Sedimenation equilibrium techniques: Multiple speed analyses and overspeed procedure, *Biophys. Chem. 5*, 185−196.
93. Thompson, P. A., Eaton, W. A., and Hofrichter, J. (1997) Laser temperature jump study of the helix → coil kinetics of an alanine peptide interpreted with a "kinetic zipper" model, *Biochemistry 36*, 9200−9210.
94. Perkins, S. J. (1986) Protein volumes and hydration effects, *Eur. J. Biochem. 157*, 168−180.
95. Durchschlag, H. (1986) in *Thermodynamic Data for Biochemistry and Biotechnology* (Hinz, H.-J., Ed.) pp 45−128, Springer-Verlag, Berlin.
96. Robertson, A. D., and Murphy, K. P. (1997) Protein structure and the energetics of protein stability, *Chem. Rev. 97*, 1251−1267.
97. Lapidus, L. J., Eaton, W. A., and Hofrichter, J. (2000) Measuring the rate of intramolecular contact formation in polypeptides, *Proc. Natl. Acad. Sci. U.S.A. 97*, 7220−7225.
98. Steinfeld, J. I., Francisco, J. S., and Hae, W. L. (1989) *Chemical Kinetics and Dynamics*, Prentice Hall, Englewood Cliffs, NJ.
99. Berne, B. J., Borkovec, M., and Straub, J. E. (1988) Classical and modern methods in reaction-rate theory, *J. Phys. Chem. 92*, 3711−3725.
100. Bieri, O., Wirz, J., Hellrung, B., Schutkowski, M., Drewello, M., and Kiefhaber, T. (1999) The speed limit for protein folding measured by triplet−triplet energy transfer, *Proc. Natl. Acad. Sci. U.S.A. 96*, 9597−9601.
101. Lapidus, L. J., Steinbach, P. J., Eaton, W. A., Szabo, A., and Hofrichter, J. (2002) Effects of chain stiffness on the dynamics of loop formation in polypeptides. Appendix: Testing a 1-dimensional diffusion model for peptide dynamics, *J. Phys. Chem. B 106*, 11628−11640.
102. Lapidus, L. J., Eaton, W. A., and Hofrichter, J. (2002) Measuring dynamic flexibility of the coil state of a helix-forming peptide, *J. Mol. Biol. 319*, 19−25.
103. Huang, F., and Nau, W. M. (2003) A conformational flexibility scale for amino acids in peptides, *Angew. Chem., Int. Ed. 42*, 2269−2272.
104. Krieger, F., Fierz, B., Bieri, O., Drewello, M., and Kiefhaber, T. (2003) Dynamics of unfolded polypeptide chains as model for the earliest steps in protein folding, *J. Mol. Biol. 332*, 265−274.
105. Huang, F., Hudgins, R. R., and Nau, W. M. (2004) Primary and secondary structure dependence of peptide flexibility assessed by fluorescence-based measurement of end-to-end collision rates, *J. Am. Chem. Soc. 126*, 16665−16675.
106. Huang, F., and Nau, W. M. (2005) Photochemical techniques for studying the flexibility of polypeptides, *Res. Chem. Intermed. 31*, 717−726.
107. Krieger, F., Moglich, A., and Kiefhaber, T. (2005) Effect of proline and glycine residues on dynamics and barriers of loop formation in polypeptide chains, *J. Am. Chem. Soc. 127*, 3346−3352.
108. Plaxco, K. W., Simons, K. T., and Baker, D. (1998) Contact order, transition state placement and the refolding rates of single domain proteins, *J. Mol. Biol. 277*, 985−994.
109. Buscaglia, M., Schuler, B., Lapidus, L. J., Eaton, W. A., and Hofrichter, J. (2003) Kinetics of intramolecular contact formation in a denatured protein, *J. Mol. Biol. 332*, 9−12.
110. Buscaglia, M., Lapidus, L. J., Eaton, W. A., and Hofrichter, J. (2006) Effect of denaturants on loop dynamics in polypeptides, *Biophys. J.* (in press).
111. Zhou, Y. Q., and Linhananta, A. (2002) Role of hydrophilic and hydrophobic contacts in folding of the second β-hairpin fragment of protein G: Molecular dynamics simulation studies of an all-atom model, *Proteins 47*, 154−162.
112. Wishart, D. S., Sykes, B. D., and Richards, F. M. (1992) The chemical-shift index: A fast and simple method for the assignment of protein secondary structure through NMR spectroscopy, *Biochemistry 31*, 1647−1651.

BI052556A